A scalable microstructure photonic coating fabricated by roll-to-roll "defects" for daytime sub-ambient passive radiative cooling

Sipan Liu[a, ‡], Chenxi Sui[b,c, ‡†], Myers Harbinson[a], Michael Pudlo[a], Himendra Perera[d], Zhenzhen Zhang[e], Ruguan Liu[f], Zahyun Ku[g], Md Didarul Islam[a], Yuxuan Liu[a], Ronghui Wu[b,c†], Yong Zhu[a], Jan Genzer[d], Saad A. Khan[d], Po-Chun Hsu[b,c†], Jong Eun Ryu[a*].*

a. Department of Mechanical and Aerospace Engineering, NC State University, Raleigh, NC, 27603, USA

b. Pritzker School of Molecular Engineering, University of Chicago, Chicago, IL, 60637, USA

c. Department of Mechanical Engineering and Materials Science, Duke University, Durham, NC, 27603, USA

d. Department of Chemical and Biomolecular Engineering, NC State University, Raleigh, NC, 27603, USA

e. Revibe Technologies, Wake Forest, NC, 27587, USA

f. Robotics department, Amazon, Inc, Westborough, MA, 01581, US

g. Materials and Manufacturing Directorate, Air Force Research Laboratory, WPAFB, OH, 45433, USA

KEYWORDS: Nanocomposite, Sub-ambient daytime cooling, Passive radiative cooling, Scalable photonic structure

ABSTRACT

The deep space's coldness (~4K) provides a ubiquitous and inexhaustible thermodynamic resource to suppress the cooling energy consumption. However, it is nontrivial to achieve sub-ambient radiative cooling during daytime under strong direct sunlight, which requires rational and delicate photonic design for simultaneous high solar reflectivity (> 94%) and thermal emissivity. A great challenge arises when trying to meet such strict photonic microstructure requirements while maintaining manufacturing scalability. Herein, we demonstrate a rapid, low-cost, template-free roll-to-roll method to fabricate spike microstructured photonic nanocomposite coatings with Al_2O_3 and TiO_2 nanoparticles embedded that possess 96.0% of solar reflectivity and 97.0% of thermal emissivity. When facing direct sunlight in the spring of Chicago (average 699 W/m^2 solar intensity), the coatings show a radiative cooling power of 39.1 W/m^2. Combined with the coatings' superhydrophobic and contamination resistance merits, the potential 14.4 % cooling energy-saving capability is numerically demonstrated across the United States.

TEXT

Climate change has severely impacted people's lives and the environment. Due to the rising temperature, approximately 20.3% of electrical energy was used in the building cooling system for the US residence and commercial buildings [1,2], presenting a challenge toward a sustainable future. Passive radiative cooling (PRC) materials can mitigate cooling consumption by delivering wireless access to the cold thermodynamic resources (~4K) in deep space [3–11]. By reflecting solar radiation and radiating heat into the cold universe through the atmospheric transparent window, the radiative cooling materials can achieve noticeable cooling energy savings under direct sunlight. The ideal radiative cooling materials should simultaneously possess high cooling power, low-cost, scalable manufacturing, and contamination resistance characteristics. Previous research showed that rough microstructures could achieve high cooling power and anti-contamination since the rough surfaces elevate the thermal emissivity by creating a gradual refractive index change and generating a superhydrophobic surface [3,12–15]. However, nontriviality arises when fabricating the desired microstructures with low-cost and scalability, because high mid-infrared (mid-IR) emissivity requires high-precision control of the photonic microstructures, where costly and low-yield nanofabrication techniques are generally employed (such as photolithography and nanoimprinting) [3,12–15]. Thus, innovative manufacturing methods need to be developed to fabricate these microstructures for large-scale applications, such as building energy saving.

Roll-to-roll has been an industrial-level process for scalable and inexpensive thin-film fabrication. *Zhai et al.* first used the roll-to-roll method to fabricate flat SiO_2/polymethylpentene nanocomposite film with a silver reflection layer to obtain a solar reflectance of 96% and a mid-infrared emissivity of 93%. However, the e-beam metal evaporation silver layer significantly

increases the manufacturing cost and time [5]. *Zhou et al.* directly coated a flat polydimethylsiloxane (PDMS) layer on the metal sheet by the roll-to-roll method, which can avoid the expensive metal evaporation process. However, the performance and cost were limited by the substrate metal [16]. The common ribbon and spike defects in traditional roll-to-roll manufacturing inspired researchers to develop a novel scalable way to fabricate periodical microstructures [17–20]. Specifically, the positive pressure gradient generated in the downstream meniscus sows the seeds of the spike "defects" on the surface [21–23]. These defects can be robustly kept when the material's rheological properties are modified by adding nanoparticles. In this situation, the defects' peak pitch length is correlated with material properties (i.e., surface energy, viscosity) and fabrication parameters (i.e., roller radius, roller gap, and roller speed) [24–26]. The optimized spike microstructures for high cooling performance can be obtained by manipulating the embedded nanoparticles and fabrication parameters. In addition, metal oxide nanoparticles can reflect sunlight due to the particles' intense backscattering [27–29], which potentially enhances the daytime radiative cooling power. Therefore, the modified roll-to-roll manufacturing method could be a cost-effective candidate for fabricating high-performance daytime radiative cooling photonic structures on a large scale.

In this study, we first demonstrated a template-free roll-to-roll method combined with polymetric nanocomposites to fabricate photonic spike coatings for daytime radiative cooling (Figure 1(a-e) and Supporting Information section 2 (SI 2) Figure S1-S2). A bilayer structure comprising Al_2O_3/polydimethylsiloxane (PDMS) and TiO_2/PDMS enhances the reflectivity of ultraviolet (UV) light (Figure 2(a))[30]. The fabricated photonic coatings show a directional emittance in mid-IR of 97.0% and a state-of-the-art substrate-independent solar radiation directional reflectance of 96.0% (Figure 2(b)). The photonic coating generates a sub-ambient cooling power as high as 39.1

W/m^2 in the daytime of Chicago with a 0.125 cloud cover ratio. The building energy modeling result shows a 14.4 % cooling system energy (31.7 GJ/year) saving capability across the U.S. Compared with the state-of-the-art radiative cooling materials (Figure 2(c), SI 3 and 4, normalized in same weather condition based on May 4th of Chicago, IL, USA), our photonics coating possesses a high solar reflectivity, thermal emissivity, and cooling power [3–8,31]. Besides, the photonic coating possesses superhydrophobic merit (water contact angle = 156^{o}), promoting contamination resistance (Figure 2(d) and Figure S3).

The ideal radiative cooling materials should possess high solar reflectivity and thermal emissivity. The transparent PDMS is used for high thermal emission. TiO_2 and Al_2O_3 nanoparticles are mixed with PDMS to enhance solar reflectivity. TiO_2 is a commercial white painting material with high reflectivity at a thin thickness due to its high refractive index (~2.7). However, the TiO_2 highly absorbs the UV and blue light due to the 3.0 eV bandgap (413 nm), which limits the solar reflectivity around 91% [32]. Therefore, low-cost Al_2O_3 nanoparticles are introduced to suppress UV absorptivity to tackle this challenge [30]. The final design of the bilayer photonic materials is shown in Figures 1(a) and 2(a). The Al_2O_3/PDMS is layered on top of the TiO_2/PDMS to prevent the UV absorption of TiO_2. Theoretically, larger backscattering coefficients of the nanoparticles lead to higher reflectivity. To validate this, the backscattering coefficients of the nanoparticles were calculated by Mie's theory (Figure 3(a-b), Figure S4, and SI 6). The selection of 500 nm-sized TiO_2 particles was based on their strong backscattering coefficient peak aligning with the peak of solar radiation at 500 nm. For the 200 nm-sized Al_2O_3 particles, they were chosen due to their high backscattering coefficient in the UV range and improved processability in PDMS compared to particles of size 100 nm.

Apart from the improved solar reflectivity, we elevated the thermal emissivity by fabricating the spike microstructures on the top surface of the coating. The spike microstructures (~30 μm lateral length) only had a negligible effect on the solar spectrum reflectivity according to Rigorous Coupled-Wave Analysis (RCWA) simulation (Figure 3(c)), because of the large mismatch between the wavelength of the incident light and the structure size (Figure 3(c) and SI 8). The spike microstructures create a gradual refractive index change at the air/coating interface, which enhances the thermal emissivity [3]. The enhancement of the thermal emissivity by the photonic microstructures was simulated by finite element analysis (FEA, COMSOL Multiphysics 5.5, SI 9). The FEA demonstrates that the microstructures significantly increase the hemisphere emissivity from 70.8% (flat PDMS, f-P) to 87.0% (triangular microstructured PDMS, t-P) at mid-IR (Figure 3(d), SI 9). The triangular microstructure also shows higher emissivity than square and circular topographies (Figure S9-S10). Boosted by the strong mid-IR absorption of Al_2O_3 or TiO_2 nanoparticles (25 vol% particle concentration), the emissivity can be promoted further to 92.9% (Figure 3(d) and Figure S11). The simulation results also reveal that the higher height and lower peak pitch length (denser) of the spike lead to a higher emissivity (Figure S12), which guides our roll-to-roll fabrication.

For cooling energy-saving applications, the radiative cooling photonic coating materials must be fabricated on a large scale. The rapid roll-to-roll method fabricates the TiO_2/PDMS and Al_2O_3/PDMS bilayer photonic coating materials with spike microstructures by employing viscoelastic fluid instability. The formation of the spike peaks is described in Figure 1(b) and Video 1 (15 vol% Al_2O_3/PDMS, relatively low viscosity material, and low roller speed were utilized for convenient photography. It is not final products). Our previous simulation research demonstrated

that surface energy γ, viscosity η *(or complex viscosity* η^**)*, roller radius R, roller gap d, and roller speed U were strongly correlated with the pressure gradient in the flow direction, which directly led to the formation of the spike "defects" [23]. To demonstrate the effects of η, U, γ, and R/d on the final spikes' peak pitch length (p_{spike}), parametric experiments are conducted with U ranging from 20 rpm to 100 rpm, and R/d from 100 to 320. The 4 - 24 vol% Al_2O_3/PDMS nanocomposites are prepared for different viscosities. The γ *and* η^* measurement results of the nanocomposites are shown in Figure 3(e-f) and SI 10. The parametric roll-to-roll experiment results demonstrate that the higher η (higher particle content), U, and R/d would lead to a smaller p_{spike} as shown in Figure 3(g) and Table S5. The Capillary number ($Ca=\eta U/\gamma$, used to be the index for predicting the critical point of the roll-to-roll defect appearance, but the fabrication in this study is far beyond the critical point) could not fit the viscoelastic fluid fabrication very well (Figure S15). We propose a novel Roll-to-roll Defects Coefficient, $RDC= ((\eta/\gamma)^{1/3} UR / d)^{-0.5}$, to fit with the p_{spike}. The p_{spike} *vs. RDC* result is shown in Figure 3(h). A linear proportion shows that the p_{spike} decreased as the *RDC* decreased.

In the final bilayer products, a flat 25 vol% TiO_2/PDMS is the first roll-to-roll fabricated and cured. Then, the top layer is fabricated on the flat layer by roll-to-roll method, where the 26 vol% Al_2O_3 and 3 vol% SiO_2 (10 nm, stabilization particles) are mixed into PDMS to achieve close-boundary viscosity but with processability. When the U went to 100 rpm and the R/d went to 320, the ~100 μm p_{spike} is achieved (Figure 1(d-e)), which is desired for improving thermal emissivity (Figure 1(d-e)).

It is necessary to characterize the optical properties of solar and mid-IR ranges to prove the radiative cooling capability of the photonic coating. The ultraviolet-visible (UV-vis) and Fourier transform infrared (FTIR) spectrometers characterize solar reflectivity and mid-IR thermal emissivity, respectively. In Figure 3(i), the UV-vis results show that the bilayer Al_2O_3/PDMS-TiO_2/PDMS coating overcomes the drawbacks of the Al_2O_3/PDMS (low overall reflectivity, 59.7% with 100 μm thickness) and TiO_2/PDMS (high absorption at UV, 91.7% solar reflectance with 100 μm thickness). A 96.0% solar reflectivity is achieved, which is comparable with PDMS/silver [33]. The FTIR measurement verified that the spike structure enhanced the mid-IR emission (Figure 3(j)). The 97.0% and 96.5% emissivity are obtained from the structured bilayer Al_2O_3/PDMS-TiO_2/PDMS and the structured TiO_2/PDMS samples, respectively. The referenced materials, flat TiO_2/PDMS and flat PDMS, achieve 95.0% and 93.2% emissivity, respectively.

To assess the daytime radiative cooling performance of the sample, a Peltier-based cooling power measurement platform was established near Michigan Lake in Chicago, IL (Figure S16). The temperature drop measurement setup was positioned on a rooftop at Chicago University, Chicago, IL (Figure S17). The outdoor measurements took place in Chicago on May 4th, 2023. The measurement system depicted in Figure 4(a-c) consisted of a Peltier device, a PID controller, a data acquisition (DAQ) system, a power supply, a thermopile pyranometer, and a device for measuring the sample temperature. The theoretical calculations were conducted based on the model proposed by *Aili (2021)* [34]. For these calculations, temperature and humidity data were obtained from field test measurements, the heat transfer coefficient was estimated as 10 W/(m^2K), and the cloud cover rate 0.125 was cited from National Oceanic and Atmospheric Administration's (NOAA) National Weather Service (NWC) – Chicago O'Hare International Airport weather

record [35]. The Al_2O_3/PDMS-TiO_2/PDMS coating demonstrated an average cooling power of 39.1 W/m² from 9:37 AM to 10:45 AM, as determined from the field test. This value was slightly lower than the theoretical calculation result of 55.1 W/m², as shown in Figure 4(d) and Figure S18. The deviation between the field test and theoretical calculation may be attributed to factors such as the estimated cloud cover rate and parasitic heat loss (heat convection and conduction) from the test platform. Regarding the temperature-drop test, the same sample exhibited an average temperature drop of 5.2°C, slightly lower than the theoretical model calculation of 6.2°C, as depicted in Figure 4(e) and Figure S18.

The infrared camera image clearly illustrates the excellent thermal emissivity of the coating, allowing for effective dissipation of the heat beneath the sample.(Figure 4(f)). To demonstrate the outdoor UV durability of the coating, one-year equivalent solar light UV radiation was applied to the coating continually. The results demonstrated no significant mechanical strength or optical properties degradation after one-year equivalent solar light UV radiation (SI 13, Figure S19-S20).

Inspired by the radiative cooling, UV resistance and self-cleaning capability, we proposed that the bilayer photonic coatings can serve as the efficient radiative coatings of the roofs for cooling energy saving in buildings (Figure 5(a)). To quantitatively assess the scale-up impact of photonic coatings on building cooling efficiency, we utilized *EnergyPlus*, incorporating experimentally measured optical properties of the materials. This allowed us to simulate the potential energy savings in cooling throughout the year for mid-rise apartments across various locations in the United States.Fifteen cities corresponding to fifteen climate zones in the U.S. were chosen to calculate the cooling energy consumption [6,33,36]. Compared with the baseline, buildings with radiative cooling roofs save energy up to 65.25 GJ/year in Phoenix, which constitutes 11.1% of the year-round cooling energy in the baseline buildings (Figure 5(b)). As shown in the cooling

energy saving map (Figure 5(c)), the cooling materials benefit more in the hot and dry areas: 54.66 GJ/year in Honolulu (Climate zone number: 1A), 45.1 GJ/year in Austin (2A), 65.24 GJ/year in Phoenix (2B) and 40.8 GJ/year in LA (3B). Even if the temperature and solar radiation are high in these areas, the radiative cooling materials perform better because they reflect sunlight nearly perfectly and radiate more heat to the deep universe. However, the saving amount gradually decreases when the cooling materials are exposed to the weather in the cold areas: 9.3 GJ/year in Fairbanks (8) and 14.5 GJ/year in Duluth (7). It is because the cooling load is small in cold weather. Since the radiative photonic coating provides all-day cooling power when space cooling is needed [33], by applying our radiative cooling photonic coatings to rooftops, an estimated average annual energy savings of approximately 31.7 GJ/year could be achieved across the entire United States. This accounts for approximately 14.4% of the total cooling energy consumed throughout the year in the United States.

In this study, we employed a cost-effective and scalable approach, the roll-to-roll method, to fabricate high-performance passive radiative cooling microstructured photonic coatings. Through careful control of the nanocomposite's viscosity and fabrication parameters such as roller gap and speeds, we successfully generated periodic spike microstructures during the roll-to-roll process. These microstructures endowed the materials with remarkable properties, including 97.0% emissivity and strong self-cleaning capability.

To predict the peak pitch length based on the viscoelastic properties of the materials and fabrication parameters, we proposed a novel metric called Roll-to-roll Defect Coefficient (RDC). The photonic coating exhibited an average cooling power of 39.1 W/m^2 under direct sunlight. Leveraging its high cooling power, scalability in fabrication, and superhydrophobic

characteristics, the coating was proposed as an effective solution for cooling roofs. Numerical simulations demonstrated a significant potential for year-round energy savings, with approximately 14.4% of building cooling energy consumption in the United States being mitigated.

Furthermore, this fabrication method is adaptable to a wide range of viscous composite pastes, enabling the scalable application of photonic coatings. The findings of this research not only offer a promising platform for expanding the application of traditional roll-to-roll fabrication but also serve as inspiration for technological advancements in radiative cooling materials.

FIGURES

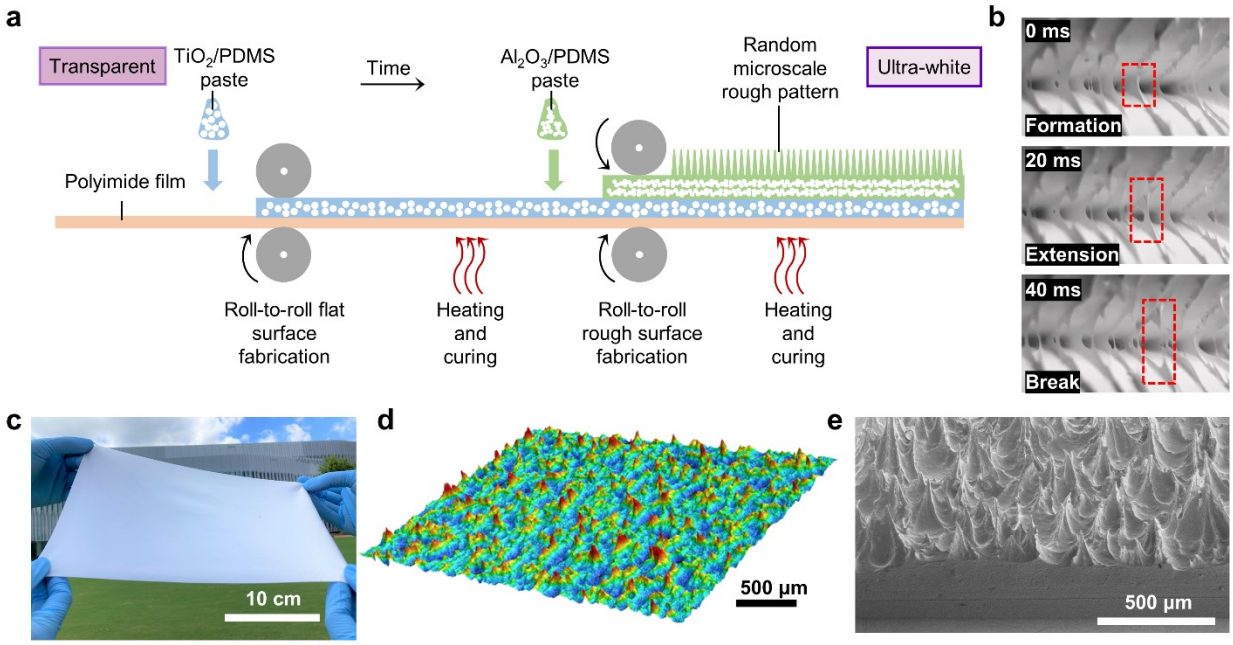

Figure 1. (a) Schematic of the bilayer nanocomposite microstructure photonic coating fabrication. (b) The spike formation schematic during the roll-to-roll fabrication process (15 vol% Al_2O_3/PDMS with relatively low viscosity and low roller speed are utilized for convenient photography, which is not final product). (c-e) The bilayer products (26 vol% Al_2O_3/PDMS - 25vol% TiO_2/PDMS) sample (c) The photonic coating photograph. (d) Laser confocal picture of the photonic coating surface. (e) SEM picture of the photonic coating with a cross-section view.

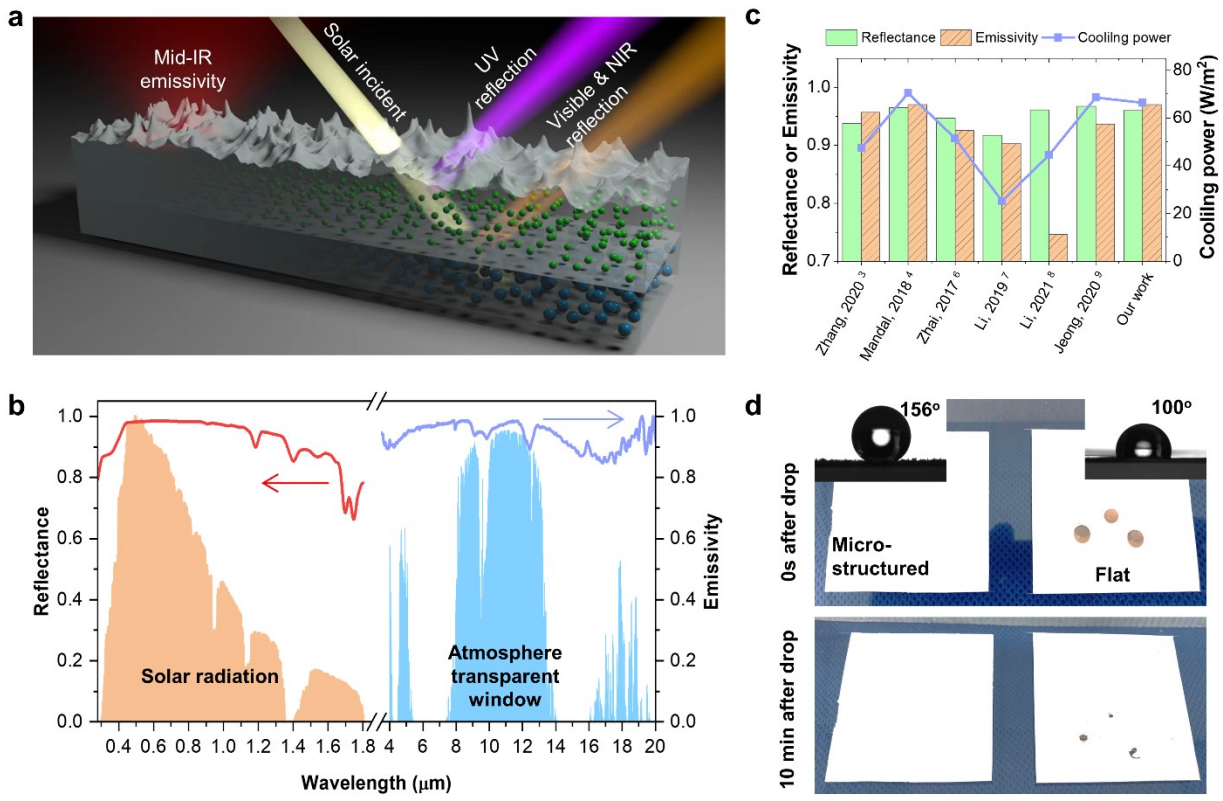

Figure 2. (a) The schematic of the bilayer photonic coating passive radiative cooling, including mid-IR emittance and separately governing the UV. The smaller green spheres are Al_2O_3, larger blue spheres are TiO_2. (b) Spectral reflectance and emissivity of the photonics coating (bilayer, thickness is 300 μm) presenting against normalized ASTM G173-03 Reference Global Tilt Solar Spectra and mid-IR transparent window of Chicago, IL, USA. (c) Comparing the solar reflectance, emissivity, and theoretical cooling power (normalized in the same ASTM G173-03 Reference Global Tilt Solar Spectra and weather condition of Chicago, IL by MODTRAN) with the state-of-the-art radiative cooling materials record in the reference [3-9]. (d) Photonic coating's superhydrophobicity (water contact angle = 156°) and contamination resistance demonstration with 30 ° slope (Side view picture is in Figure S3).

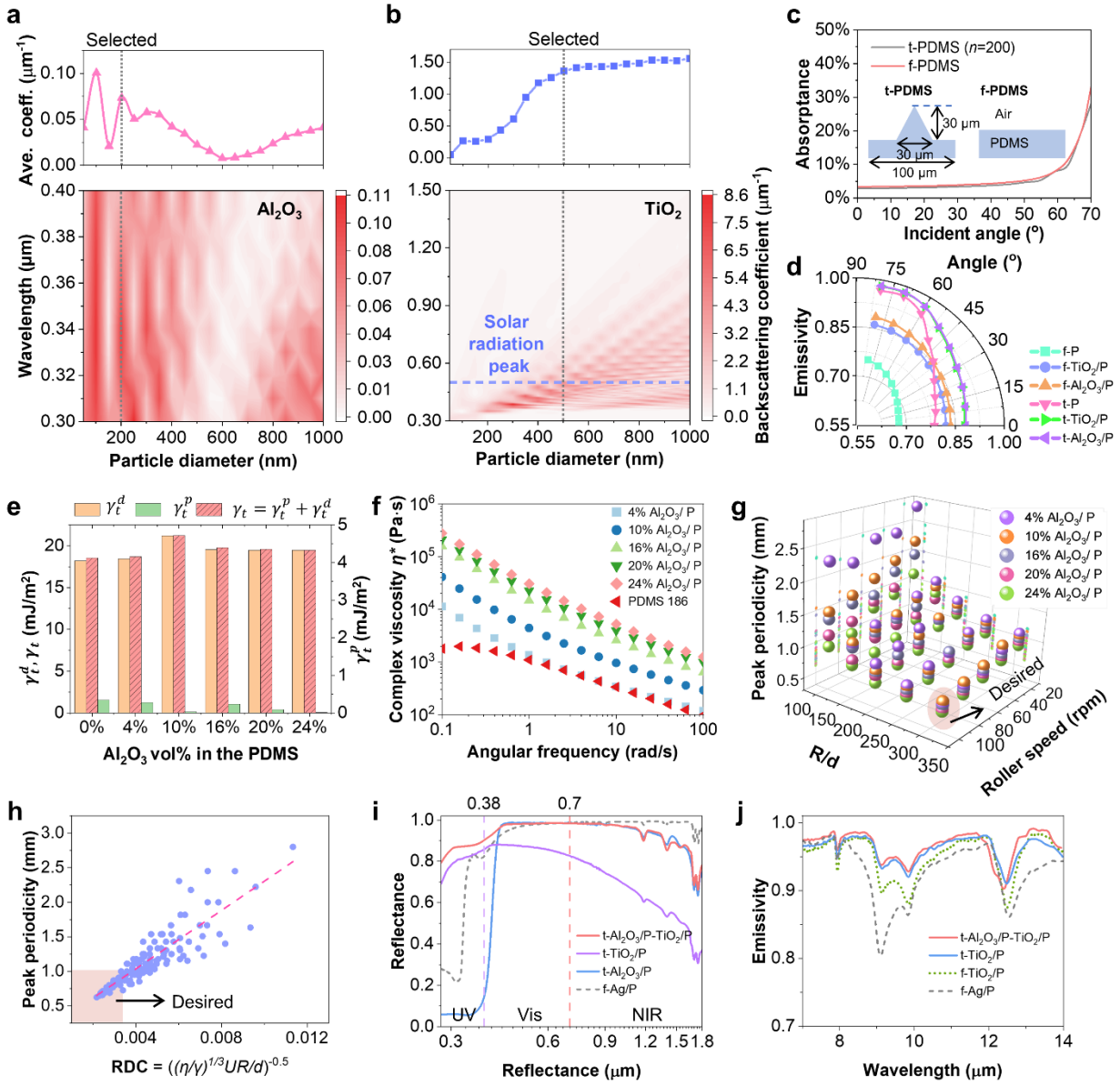

Figure 3. (a-b) The nanoparticle/PDMS backscattering coefficients calculation by Mie's theory (particles concentrations were 25 vol%, "Selected" marked the particles size in final product). (a) The Al_2O_3 nanoparticles' average backscattering coefficient, and the backscattering coefficient along the change of the particle diameter and wavelength at UV range, (b) The TiO_2 nanoparticles' average backscattering coefficient, and the backscattering coefficient along the change of the particle diameter and wavelength at solar spectra range. (c) The spike microstructure's effect on

solar spectral reflectance, and the models in the RWAC model. In the legend, t- is a triangular spike model, and f- is the flat model. (d) The enhancement results for the mid-IR emissivity by the photonic microstructures simulated by finite elements analysis (FEA, COMSOL, particles concentration was 25 vol%. In the legend, P is PDMS. (e) The surface energy components (polar, γ_t^d, disperse, γ_t^p, total, $\gamma_t = \gamma_t^p + \gamma_t^d$) of the different Al_2O_3 (200 nm) particle concentrations in PDMS (P). (f) Complex viscosity (η^*) vs. angular frequency. (g) A parametric experiment of the nanocomposite pastes, Peaks pitch length (p_{peak}) *vs.* Roller geometry factor (*R/d*) and roller speed (*U*). (h) Peak pitch length *vs.* Roll-to-roll defects coefficient (RDC). (i) The reflectance of a photonic coating sample (t- Al_2O_3/P-TiO_2/P) and other comparing samples on the solar spectrum. (j) The emissivity of the photonic coating and other comparing samples at mid-IR (7-14 μm). In the legend, t- is spike microstructured coating, f- is the flat coating, P is PDMS.

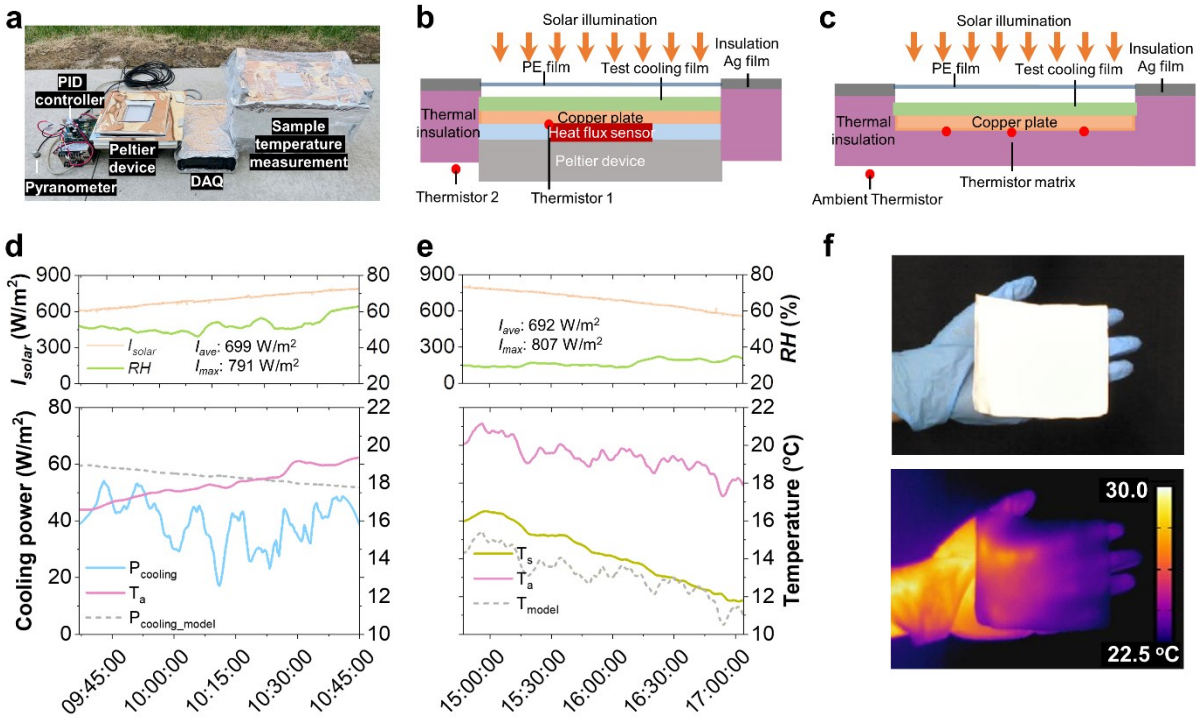

Figure 4. (a) Outdoor cooling power and temperature-drop measurement platforms. (b) Schematic of the Peltier-based measurement platform. (c) Schematic of the temperature-drop measurement platform. (d) The bilayer photonic coatings cooling power ($P_{cooling}$) measurement result and theoretical model prediction cooling power ($P_{cooling\_model}$) with corresponding relative humidity (RH), ambient temperature (T_a), and solar illumination, ($I_{solar,}$ average and maximum illumination are I_{ave} and I_{max}, respectively). (e) The bilayer photonic coatings temperature measurement result (T_s) and model predicted temperature (T_{model}) with corresponding RH, T_a, and I_{solar}. (f) The infrared thermal camera pictures of bilayer photonic coating on the author's hand.

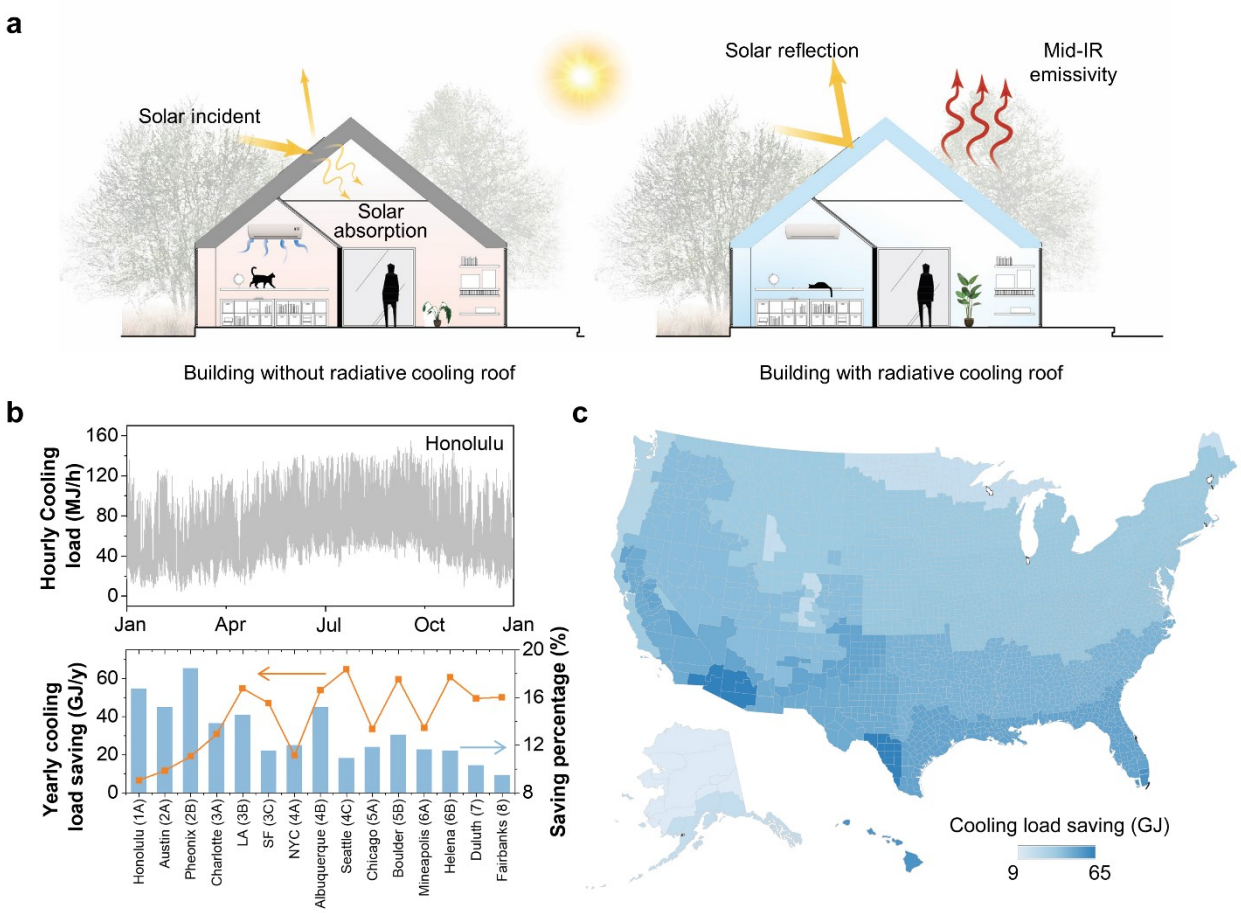

Figure 5. (a) Schematic of the photonic coating applied on building cooling. (b) Building cooling energy saving simulation results in 15 cities corresponding to 15 climate zones in the US compared with the baseline buildings (Honolulu as 1A climate zone example). (c) The cooling energy saving map of the US.

ASSOCIATED CONTENT

Supporting Information.

The following files are available free of charge.

Video 1: The spikes' formation slow-motion movie. (MP4)

Supplementary material: Additional experimental details, materials, and methods, including photographs of experimental setup. (PDF)

AUTHOR INFORMATION

Corresponding Author

* Po-Chun Hsu, Email: pochunhsu@uchicago.edu; Jong Eun Ryu, Email: jryu@ncsu.edu

Present Addresses

† Present address: Chenxi Sui, Ronghui Wu, and Po-Chun Hsu: Pritzker School of Molecular Engineering, University of Chicago, Chicago, IL, 60637, USA.

Author Contributions

The manuscript was written through contributions of all authors. All authors have given approval to the final version of the manuscript. ‡These authors contributed equally.

Funding Sources

National Science Foundation, No. 2031558. (Jong E. Ryu)

National Science Foundation (No. ECCS-2025064).

ACKNOWLEDGMENT

This research is based upon work supported by the start-up fund by Pratt School of Engineering, Duke University (P. Hsu), NCSU Faculty Research and Professional Development award (J. Ryu), and National Science Foundation under grant No. 2031558. Part of this work was performed at the Analytical Instrumentation Facility (AIF) at North Carolina State University, supported by the State of North Carolina and the National Science Foundation (award number ECCS-2025064).

ABBREVIATIONS

PRC, Passive radiative cooling; Mid-IR, Mid-infrared; PDMS, Polydimethylsiloxane; RCWA, Rigorous Coupled-Wave Analysis; FEA, Finite element analysis; RDC, Roll-to-roll Defects Coefficient; UV-Vis, ultraviolet-visible (UV-vis); FTIR, Fourier transform infrared.

REFERENCES

(1) US Department of Energy. 2010 Residential Energy End-Use Expenditure Splits, by Fuel Type. *Build. Energy Data B.* **2012**.

(2) Chu, S.; Majumdar, A. Opportunities and Challenges for a Sustainable Energy Future. *Nature* **2012**, *488* (7411), 294–303.

(3) Zhang, H.; Ly, K. C. S.; Liu, X.; Chen, Z.; Yan, M.; Wu, Z.; Wang, X.; Zheng, Y.; Zhou, H.; Fan, T. Biologically Inspired Flexible Photonic Films for Efficient Passive Radiative Cooling. *Proc. Natl. Acad. Sci. U. S. A.* **2020**, *117* (26), 14657–14666. https://doi.org/10.1073/pnas.2001802117.

(4) Mandal, J.; Fu, Y.; Overvig, A. C.; Jia, M.; Sun, K.; Shi, N. N.; Zhou, H.; Xiao, X.; Yu, N.; Yang, Y. Hierarchically Porous Polymer Coatings for Highly Efficient Passive Daytime Radiative Cooling. *Science* **2018**, *362* (6412), 315–319.

https://doi.org/10.1126/science.aat9513.

(5) Zhai, Y.; Ma, Y.; David, S. N.; Zhao, D.; Lou, R.; Tan, G.; Yang, R.; Yin, X. Scalable-Manufactured Randomized Glass-Polymer Hybrid Metamaterial for Daytime Radiative Cooling. *Science* **2017**, *355* (6329), 1062–1066. https://doi.org/10.1126/science.aai7899.

(6) Li, T.; Zhai, Y.; He, S.; Gan, W.; Wei, Z.; Heidarinejad, M.; Dalgo, D.; Mi, R.; Zhao, X.; Song, J.; Dai, J.; Chen, C.; Aili, A.; Vellore, A.; Martini, A.; Yang, R.; Srebric, J.; Yin, X.; Hu, L. A Radiative Cooling Structural Material. *Science* **2019**, *364* (6442), 760–763. https://doi.org/10.1126/science.aau9101.

(7) Li, D.; Liu, X.; Li, W.; Lin, Z.; Zhu, B.; Li, Z.; Li, J.; Li, B.; Fan, S.; Xie, J.; Zhu, J. Scalable and Hierarchically Designed Polymer Film as a Selective Thermal Emitter for High-Performance All-Day Radiative Cooling. *Nat. Nanotechnol.* **2021**, *16* (2), 153–158. https://doi.org/10.1038/s41565-020-00800-4.

(8) Jeong, S. Y.; Tso, C. Y.; Wong, Y. M.; Chao, C. Y. H.; Huang, B. Daytime Passive Radiative Cooling by Ultra Emissive Bio-Inspired Polymeric Surface. *Sol. Energy Mater. Sol. Cells* **2020**, *206* (July 2019), 110296. https://doi.org/10.1016/j.solmat.2019.110296.

(9) Raman, A. P.; Anoma, M. A.; Zhu, L.; Rephaeli, E.; Fan, S. Passive Radiative Cooling below Ambient Air Temperature under Direct Sunlight. *Nature* **2014**, *515* (7528), 540–544. https://doi.org/10.1038/nature13883.

(10) Hsu, P.-C.; Song, A. Y.; Catrysse, P. B.; Liu, C.; Peng, Y.; Xie, J.; Fan, S.; Cui, Y. Radiative Human Body Cooling by Nanoporous Polyethylene Textile. *Science* **2016**, *353* (6303), 1019–1023.

(11) Leroy, A.; Bhatia, B.; Kelsall, C. C.; Castillejo-Cuberos, A.; Di Capua H, M.; Zhao, L.; Zhang, L.; Guzman, A. M.; Wang, E. N. High-Performance Subambient Radiative Cooling Enabled by Optically Selective and Thermally Insulating Polyethylene Aerogel. *Sci. Adv.* **2019**, *5* (10), eaat9480.

(12) Shi, N. N.; Tsai, C. C.; Camino, F.; Bernard, G. D.; Yu, N.; Wehner, R. Keeping Cool: Enhanced Optical Reflection and Radiative Heat Dissipation in Saharan Silver Ants. *Science* **2015**, *349* (6245), 298–301. https://doi.org/10.1126/science.aab3564.

(13) Smith, G. B.; Gentle, A. R.; Arnold, M. D.; Gali, M. A.; Cortie, M. B. The Importance of Surface Finish to Energy Performance. *Renew. Energy Environ. Sustain.* **2017**, *2*, 13.

(14) Wang, T.; Wu, Y.; Shi, L.; Hu, X.; Chen, M.; Wu, L. A Structural Polymer for Highly Efficient All-Day Passive Radiative Cooling. *Nat. Commun.* **2021**, *12* (1), 365.

(15) Song, J.; Seo, J.; Han, J.; Lee, J.; Lee, B. J. Ultrahigh Emissivity of Grating-Patterned PDMS Film from 8 to 13 μ m Wavelength Regime. *Appl. Phys. Lett.* **2020**, *117* (9), 94101.

(16) Zhou, L.; Song, H.; Liang, J.; Singer, M.; Zhou, M.; Stegenburgs, E.; Zhang, N.; Xu, C.; Ng, T.; Yu, Z. A Polydimethylsiloxane-Coated Metal Structure for All-Day Radiative Cooling. *Nat. Sustain.* **2019**, *2* (8), 718–724.

(17) Castillo, M. E. G.; Patera, A. T. Three-Dimensional Ribbing Instability in Symmetric Forward-Roll Film-Coating Processes. *J. Fluid Mech.* **1997**, *335*, 323–359.

(18) Chong, Y. H.; Gaskell, P. H.; Kapur, N. Coating with Deformable Rolls: An Experimental Investigation of the Ribbing Instability. *Chem. Eng. Sci.* **2007**, *62* (15), 4138–4145.

(19) Bauman, T.; Sullivan, T.; Middleman, S. Ribbing Instability in Coating Flows: Effect of Polymer Additives. *Chem. Eng. Commun.* **1982**, *14* (1–2), 35–46.

(20) Greener, J.; Sullivan, T.; Turner, B.; Middleman, S. Ribbing Instability of a Two-Roll Coater: Newtonian Fluids. *Chem. Eng. Commun.* **1980**, *5* (1–4), 73–83.

(21) Abbasi, S.; Zebarjad, S. M.; Baghban, S. H. N.; Youssefi, A.; Ekrami-Kakhki, M.-S. Experimental Investigation of the Rheological Behavior and Viscosity of Decorated Multi-Walled Carbon Nanotubes with TiO2 Nanoparticles/Water Nanofluids. *J. Therm. Anal. Calorim.* **2016**, *123* (1), 81–89.

(22) Jo, B.; Banerjee, D. Viscosity Measurements of Multi-Walled Carbon Nanotubes-Based High Temperature Nanofluids. *Mater. Lett.* **2014**, *122*, 212–215.

(23) Islam, M. D.; Perera, H.; Black, B.; Phillips, M.; Chen, M.; Hodges, G.; Jackman, A.; Liu, Y.; Kim, C.; Zikry, M. Template-Free Scalable Fabrication of Linearly Periodic Microstructures by Controlling Ribbing Defects Phenomenon in Forward Roll Coating for Multifunctional Applications. *Adv. Mater. Interfaces* **2022**, 2201237.

(24) Fields, R. J.; Ashby, M. F. Finger-like Crack Growth in Solids and Liquids. *Philos. Mag.* **1976**, *33* (1), 33–48.

(25) Lee, J. H.; Han, S. K.; Lee, J. S.; Jung, H. W.; Hyun, J. C. Ribbing Instability in Rigid and Deformable Forward Roll Coating Flows. *Korea-Australia Rheol. J.* **2010**, *22* (1), 75–80.

(26) Grillet, A. M.; Lee, A. G.; Shaqfeh, E. S. G. Observations of Ribbing Instabilities in Elastic Fluid Flows with Gravity Stabilization. *J. Fluid Mech.* **1999**, *399*, 49–83.

(27) Bohren, C. F.; Huffman, D. R. *Absorption and Scattering of Light by Small Particles*; John Wiley & Sons, 2008.

(28) Li, D.; Liu, X.; Li, W.; Lin, Z.; Zhu, B.; Li, Z.; Li, J.; Li, B.; Fan, S.; Xie, J. Scalable and Hierarchically Designed Polymer Film as a Selective Thermal Emitter for High-Performance All-Day Radiative Cooling. *Nat. Nanotechnol.* **2021**, *16* (2), 153–158.

(29) Mandal, J.; Fu, Y.; Overvig, A. C.; Jia, M.; Sun, K.; Shi, N. N.; Zhou, H.; Xiao, X.; Yu, N.; Yang, Y. Hierarchically Porous Polymer Coatings for Highly Efficient Passive Daytime Radiative Cooling. *Science* **2018**, *362* (6412), 315–319. https://doi.org/10.1126/science.aat9513.

(30) Mandal, J.; Yang, Y.; Yu, N.; Raman, A. P. Paints as a Scalable and Effective Radiative Cooling Technology for Buildings. *Joule* **2020**, *4* (7), 1350–1356.

(31) Li, X.; Peoples, J.; Yao, P.; Ruan, X. Ultrawhite BaSO4Paints and Films for Remarkable Daytime Subambient Radiative Cooling. *ACS Appl. Mater. Interfaces* **2021**, *13* (18), 21733–21739. https://doi.org/10.1021/acsami.1c02368.

(32) Yu, X.; Chan, J.; Chen, C. Review of Radiative Cooling Materials: Performance Evaluation and Design Approaches. *Nano Energy* **2021**, *88* (January), 106259. https://doi.org/10.1016/j.nanoen.2021.106259.

(33) Li, X.; Sun, B.; Sui, C.; Nandi, A.; Fang, H.; Peng, Y.; Tan, G.; Hsu, P. C. Integration of Daytime Radiative Cooling and Solar Heating for Year-Round Energy Saving in Buildings. *Nat. Commun.* **2020**, *11* (1), 1–9. https://doi.org/10.1038/s41467-020-19790-x.

(34) Aili, A.; Yin, X.; Yang, R. Global Radiative Sky Cooling Potential Adjusted for Population Density and Cooling Demand. *Atmosphere (Basel).* **2021**, *12* (11), 1379.

(35) *National Weather Service*. https://www.weather.gov/wrh/Climate?wfo=lot (Accessed on May 4th, 2023), Chicago O'Hare international airport weather record.

(36) Baechler, M. C.; Williamson, J. L.; Gilbride, T. L.; Cole, P. C.; Hefty, M. G.; Love, P. M. *Building America Best Practices Series: Volume 7.1: Guide to Determining Climate Regions by County*; Pacific Northwest National Lab.(PNNL), Richland, WA (United States), 2010.

For Table of Contents Only

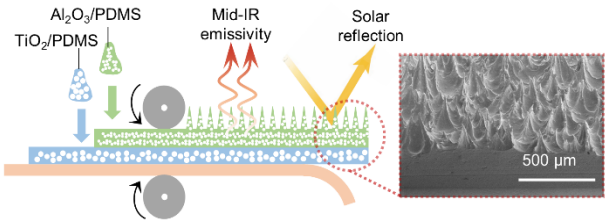

Template-free roll-to-roll passive radiative cooling coating